IEEE Open Journal of Signal Processing

Received 18 September 2022; revised 28 December 2022; accepted 28 December 2022. Date of publication 9 January 2023; date of current version 31 January 2023. The review of this article was arranged by Associate Editor U. A Khan.

Digital Object Identifier 10.1109/OJSP.2023.3235245

A Robust Indoor Localization Method for NLOS Environments Utilizing Sensor Subsets

KEIGO ISHIDA[1], EIJI OKAMOTO[1] (Member, IEEE), AND HUAN-BANG LI[2]

[1]Department of Electrical and Mechanical Engineering, Nagoya Institute of Technology, 466-8555 Nagoya, Japan
[2]National Institute of Information and Communications Technology, 239-0847 Yokosuka, Japan

CORRESPONDING AUTHOR: EIJI OKAMOTO (e-mail: okamoto@nitech.ac.jp)

ABSTRACT Indoor location localization using the time of arrival (TOA) of ultra-wideband (UWB) radio waves faces a challenge in obtaining accurate TOA values in a non-line-of-sight (NLOS) environment owing to obstacles and multipath reception. The accuracy of localization using such sensor data in an NLOS environment is significantly degraded. To address this problem in NLOS environment, we proposed a new localization method that utilizes different sensor combinations for estimation and sensor placement topology. Based on the conventional localization method using various combinations of sensors, the estimation results containing an NLOS ranging value were first removed. Subsequently, we introduced a new parameter called the topological expectancy of localization accuracy (TELA), which represents the effect of sensor placement on the accuracy of localization. The final estimation result was then obtained using the weighted average of the remaining localization results obtained by TELA. Computer simulations and experimental results showed that the performance of the proposed method is superior by 4 to 37% compared with that of conventional methods, even in the presence of many NLOS environment sensors.

INDEX TERMS Indoor localization, NLOS, TOA, cramer-rao lower bound, topological expectancy of localization accuracy (TELA).

I. INTRODUCTION

With the recent development of automated factories and distribution warehouses, accurate indoor position information is becoming increasingly important [1]. Because global navigation satellite systems (GNSS) cannot be used for indoor positioning, suitable indoor positioning methods that use radio waves have been investigated [2]. Localization with Wi-Fi [3] and Bluetooth [4] are among the most representative examples. Various signal processing methods, such as time of arrival (TOA) [5], which estimates the distance based on the propagation time of radio waves; time difference of arrival (TDOA) [6], which uses the arrival time difference of radio waves from the same transmitter; and angle of arrival (AOA) [7], which uses the arrival angle of radio waves, are widely used. In addition, the received signal strength indication (RSSI) method [8], [9], [10], which obtains distance information from the amount of power attenuation for location estimation, and the fingerprint method [11], which utilizes the location dependency of channel state information (CSI) and RSSI from multiple base stations, have also been investigated. In particular, the TOA method that uses ultra-wideband (UWB) has attracted attention because of its superior ranging accuracy and low power consumption [12], [13]. Although these methods are highly accurate in line-of-sight (LOS) environments, which exhibit good visibility, it generally degrades in non-line-of-sight (NLOS) environments [14], [15], where visibility between sensor nodes and targets is blocked. This is because the ranging value in the NLOS environment is larger than the true value owing to the reception of reflected waves.

In general, localization in NLOS environments can be approached in two ways. One is identification and removal of the ranging values of the sensors in an NLOS environment. The second is inclusion of these sensors for localization. The latter is generally called multipath-assisted indoor navigation and tracking (MINT) [16], [17], [18], which enables accurate localization even in NLOS environments by

modeling multipath components. However, in principle, these systems require a priori information called floor plans, which may be difficult to implement in cases where estimation of many areas, such as large factories or shopping malls with moving objects, is required. In comparison, the elimination methods of sensors in the NLOS environment for localization do not require prior knowledge and are relatively easy to implement. Considering this advantage, this study focuses on methods that identify and remove the ranging values of NLOS environment sensors. Hereafter, we refer to a sensor in an LOS environment as an "LOS node" and a sensor in an NLOS environment as an "NLOS node."

Many methods of reducing the impact of NLOS nodes have been studied using either CSI of the received radio wave or distance data only. Recently, regulations for UWB wireless systems have been revised for facilitating UWB usage [19], and the cost of UWB devices is expected to reduce and the use of UWB terminals is expected to increase. Therefore, this study examines a location estimation algorithm that can be applied to UWB localization systems containing a large number of UWB devices.

In conventional methods [20], [21], [22], [14], [23], [24], [25], [26], [27], [28], [29], [30], [31], [29], [32], [33], [34], localization is performed by combining distance information obtained from a large number of sensors in various ways. Furthermore, the accuracy is improved by employing localization results based on sensor combinations that do not include the distance measured by NLOS nodes. However, the accuracy of localization tends to be poor owing to the low removal accuracy of NLOS nodes [14], [15]. In this paper, we proposed a new method that improves the accuracies of NLOS node removal and localization by weighted averaging of the estimation results from sensor combinations. The contributions of this study are as follows:

The sensor combination method uses both the difference between the measured and the estimated distance (defined as *residual*), which is a conventional metric, and confidence level based on the residuals for increasing the reliability of NLOS node removal.

IN line with AOA systems, we introduced a new parameter, the topological expectancy of localization accuracy (TELA), which evaluates the accuracy of the estimated location based on the positional relationship between the sensor and estimated position and proposed an algorithm for more accurately estimating the position using the weighted average by TELA.

The remainder of this paper is organized as follows. In Section II, related studies on NLOS countermeasures for conventional UWB localization are presented. In Section III, the proposed method is extensively described, and in Section IV, the performance of the proposed method is compared with that of the conventional methods using numerical simulations. In Section V, the computational complexity and Cramer-Rao lower bound (CRLB) are derived. In Section VI, the experimental results of the proposed method using UWB sensors are evaluates, and in Section VII, conclusions are summarized.

II. RELATED WORKS

Existing methods of reducing the impact of NLOS on localization accuracy can be classified into two main categories: with and without prior knowledge [20], [21].

Those with prior knowledge are either range-[22], [23] or channel-based. A range-based method uses a known range error model and tendency. Furthermore, probability density functions (PDFs) are used for probabilistically discriminating LOS/NLOS or a predefined threshold of a metric such as the variance of the ranging value is used for discriminating LOS/NLOS. However, accurately determining the ranging errors in advance is generally difficult. Channel-based methods use channel impulse response (CIR) to determine whether the environment is NLOS and can be further divided into two categories: one uses the cumulative distribution function (CDF) of the received power distribution [23] and the other uses the signal-to-noise ratio (SNR), kurtosis, or the mean excess delay (MED) of the CIR [24], [25]. However, these methods require coupling probabilities and thresholds. However, obtaining accurate CIRs a priori and determining the appropriate thresholds by computing joint distribution functions are usually difficult.

Estimation methods that do not use prior knowledge include robust statistics [26], [27], [28], [29], mathematical programming [30], [31], [29], identification and discarding [32], [33], and location-based methods [34], [35]. Robust statistics, such as M-estimation [26], [27], which considers NLOS as an outlier and uses a robust function to minimize the effects of NLOS, and the least median square (LMedS) method [28], [29], which obtains the median of the smallest squared residuals of candidate estimates, directly mitigate the effects of NLOS without explicit NLOS discrimination. Mathematical programming includes quadratic programming, linear programming, and interior point optimization. The effect of NLOS is reduced by solving mathematical programming with constraints on the ranging values of NLOS sensors. In the identification and discard method, NLOS sensors are identified and discarded; thus, they are not used for localization. Although these methods do not require prior knowledge, they generally require many measurements and incur high computational costs.

Identification and discarding of NLOS sensors is based on feedback obtained from the localization results. On one hand, location-based methods often have lower estimation accuracy than quasi-maximum likelihood methods. The latter requires prior knowledge, whereas the former does not require prior knowledge and can improve performance with only the given measurements. Therefore, this study focuses on location-based methods, and the proposed method belongs to the NLOS identification and discard category and location-based method. A location-based method discriminates NLOS in following two ways: using residuals and reliability of ranging values. The residual is the difference between the estimated distance calculated by the estimated position and sensor nodes, and the measured distance is obtained by ranging the same location and sensors. The iterative minimum residual (IMR) method [34] typically uses

the residuals. In the IMR method, the sum of squares of the residuals is calculated for each localization, and any sensor combination with a large sum is considered to contain an NLOS sensor and is eliminated. In general, these methods use the property of fact that the residuals from sensor combinations that include NLOS sensors become large. However, this principle has some exceptions; in particular, when multiple NLOS sensors are included, the discrimination accuracy based on the residual sums significantly decreases.

On the other hand, no error model information and reduced complexity (NEMIRC) method [35], which uses the reliability of ranging values, has been proposed as a location-based method. In the NEMIRC, all sensor combinations are used for localization, and the average of the estimated positions where the reliability exceeds a threshold is used as the final estimated position. Here, reliability is defined as the minimum value of the measured distance subtracted by the estimated distance of the sensor that was not used for localization. In principle, the measurement error is positively biased and the reliability value becomes positive. Then, by eliminating the estimated positions that violate this principle, that is, a sensor node with a negative reliability value, highly accurate NLOS discrimination is achieved. In addition, NEMIRC does not uniquely determine the final localization result but rather averages multiple localization results from multiple sensor combinations, which makes it robust and less sensitive to the inclusion of some incorrectly estimated positions. However, because of the NEMIRC principle, the effect of NLOS sensor errors cannot be completely eliminated and the estimation accuracy of NLOS sensors inevitably degrades. Therefore, further improvements in the estimation accuracy of location-based methods are expected.

The proposed method is based on NEMIRC, in which a simple average of the estimated positions selected by the threshold is used as the final localization result. However, in this study, a weighted average of the estimated positions weighted according to the confidence level was applied for improving the accuracy of the localization. Several indices have been proposed in conventional studies for evaluating the confidence level of the estimated location [36], [37], [38], [39], and evaluating it based on the relationship between the placement of sensors and estimated location is common. Among these, the geometric dilution of precision (GDOP) [36] uses prior knowledge of the ranging error model and can be applied to the optimal combination of satellites for GNSS [37] and optimization of sensor placement for indoor positioning [38]. However, these methods cannot be used without prior knowledge of the channel model, as in that proposed in the present study. Another method that uses topology without prior knowledge was proposed using distance vector hop (DV-Hop) [39]. Although this method is effective in range-free schemes that do not require distance measurements, it is ineffective in methods that use ranging values. Therefore, this paper proposes a new TELA that does not require a channel model and can evaluate the reliability of the estimated position based only on the positional relationship between the sensor and estimated position. We used the proposed TELA as a weighted average of the estimated positions in the final localization result for improving performance.

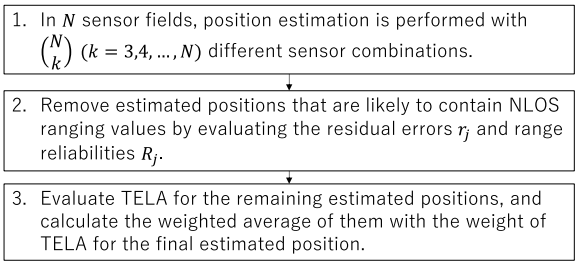

FIGURE 1. Algorithm overview of proposed method.

III. PROPOSED LOCALIZATION METHOD

The proposed method can be divided into two procedures: repeating the localization using various sensor combinations and classifying them; and calculating TELA and performing weighted average. Fig. 1 shows a flowchart of the proposed algorithm when the number of sensors in a target field is N. Steps 1–2 and 3 in Fig. 1 are described in III-A and -B, respectively.

A. LOCALIZATION WITH VARIOUS SENSOR COMBINATIONS AND SORTING OF THE RESULTS

In Step 1, as shown in Fig. 1, we first estimated the target position using all combinations of sensors. For estimating the positions for all combinations using $k = (34, \ldots, N)$ sensors by multilateration, the total number of combinations M can be calculated as

$$M = \sum_{k=3}^{N} \binom{N}{k} \tag{1}$$

In this study, the TOA [40] measurement method for UWB was assumed and time synchronization among sensors was assumed to have been obtained. In addition, the minimum value of k was set to three because multilateration requires at least three sensors. When the ranging values of k sensors are $\hat{d}_i$ $(i = 12, \ldots, k)$, the optimal estimated position is obtained by the following least-squares (LS) problem [41]:

$$(\bar{x}_j, \bar{y}_j) = \underset{\bar{x}\prime,\bar{y}\prime}{\operatorname{argmin}} \sum_{i=1}^{k} \left(\hat{d}_i - \sqrt{(x_i - \bar{x}\prime)^2 + (y_i - \bar{y}\prime)^2} \right)^2, \tag{2}$$

where $(\bar{x}_j, \bar{y}_j)$ is the j-th $(j = 12, \ldots, M)$ estimated position, $(\bar{x}_i, \bar{y}_i)$ are the coordinates of the i-th sensor in the j-th sensor combination. Eq. (2) is a nonlinear optimization problem that is generally solved using optimization methods such as the Newton-Raphson method [42]. However, in this study, the linear least squares (LLS) [43] method with a lower calculation complexity was used. Although LLS is less accurate than other nonlinear methods, it is suitable for the

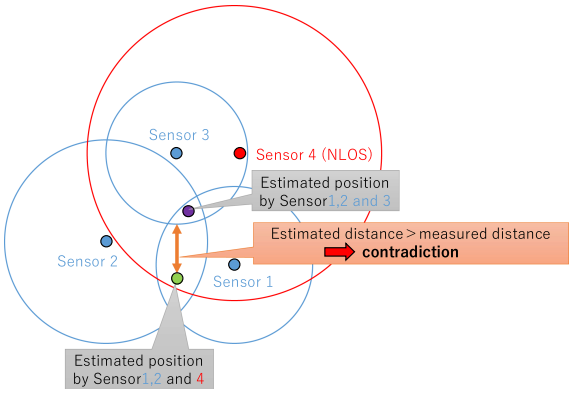

FIGURE 2. Reliability of ranging value.

proposed method because an iterative calculation of (2) for many combinations of M is required in the proposed method.

In Step 2, we evaluated the residuals and reliability of the ranging values and removed the estimated positions that were likely to include NLOS ranging values. The residual value r_j for j-th estimated position is given by the averaged squared value using the measured distance value $\hat{d}_i$ as

$$r_j = \frac{1}{k}\sum_{i=1}^{k}\left(\hat{d}_i - \sqrt{\left(x_i - \bar{x}_j\right)^2 + \left(y_i - \bar{y}_j\right)^2}\right)^2 \tag{3}$$

Then, an empirical threshold of $\delta = 0.3\ \mathrm{m}^2$ was adopted for r_j for discriminating NLOS environments, and the estimated positions with $r_j > \delta$ were removed as they were likely to contain NLOS ranging values. The optimization of δ is presented in Appendix A.

The reliability of the ranging value of j-th estimated position is defined in NEMIRC [35] as

$$R_j = \min_{l \in L}\left\{\hat{d}_l - \bar{d}_l\right\}, \tag{4}$$

where $L = \{k+1, k+2, \ldots, N\}$ is the set of sensors that are not used for localization of j-th estimation, and $\bar{d}_l$ is the estimated distance between j-th estimated position and l-th ($l \in L$) sensor and is given by

$$\bar{d}_l = \sqrt{\left(x_l - \bar{x}_j\right)^2 + \left(y_l - \bar{y}_j\right)^2} \tag{5}$$

Similar to the residuals, a threshold value $\tau = 0$ m was set for R_j. The estimated positions satisfying $R_j < \tau$ were considered to contain NLOS ranging values and were eliminated. Note that the residuals calculated in (3) and the reliability calculated in (4) are similar but different. An example of the principle that the reliability defined in (4) contributes to NLOS determination is shown in Fig. 2. The localization result from sensors 1, 2, and 3 in the LOS environment is inside the ranging distance circles of the three nodes and also inside that of the fourth sensor, which is complementary. This implies that the estimated distance is generally smaller than the ranging value. If the estimated position is assumed to be near the actual position, the estimated distance is approximately equal to the true distance and the fact that the ranging value is larger than the estimated distance value reasonably holds. However, the result of localization using sensors 1, 2, and 4 indicates that the estimated distance is larger than the ranging distance for sensor 3, which is complementary. If this estimation result is correct, the estimated distance, which corresponds to the true distance, is larger than the ranging value for sensor 3, and the ranging difference defined by (4) becomes negative for $l = 3$. This contradicts the fact that the ranging error is principally positive and is therefore an erroneous result. Therefore, the reliability of the ranging values calculated by (4) is shown to be a useful metric for determining the incorrect estimated location because of NLOS ranging values [37].

To reduce the calculation complexity, the proposed method does not consider the sensor combinations, the subsets of which are judged to contain NLOS ranging values for the rest k-process. For example, in a field with four sensors, if the combination of sensors 1, 2, and 3 is judged to be in the NLOS environment, the combination of sensors 1, 2, 3, and 4 was also considered to contain NLOS ranging values. Therefore, they were excluded from the search process. Thus, the amount of calculation was reduced, and the accuracy of NLOS discrimination was improved by reducing the possibility of misjudgment. The number of remaining estimated positions is denoted as M_{LOS}.

In real environments, partial LOS or NLOS sensors that frequently switch between LOS and NLOS environments owing to mobility objects, etc. may exist. In these environments, the proposed method measures instantaneous range values, and the localization algorithm does not take much time. Therefore, the proposed method can treat these sensors as instantaneous LOS or NLOS sensors and does not have a significant negative impact on the estimation accuracy.

B. TOPOLOGICAL EXPECTANCY OF LOCALIZATION ACCURACY

Finally, in Step 3, TELA was calculated for the remaining estimated positions $j \in M_{LOS}$, and the weighted average of these positions was used as the final localization result. TELA is defined as a scalar value, and the higher the value, the higher the localization accuracy. TELA is composed of three elements: an aspect ratio a of the polygon, the vertices of which are the sensors to be used, a distance bias b_d from the estimated position to the sensors to be used, and an angle bias b_θ formed by the straight line drawn from the estimated position of each sensor. These elements were adopted as a result of heuristic considerations. Note that because this position estimation method is a nonlinear optimization problem, we believe applying empirical factors to some extent, such as hyperparameters in machine learning, was necessary to compose TELA. The details of this process are described below.

1) ASPECT RATIO

One of the conditions for trilateration is that the sensors should not be placed on the same line for uniquely determining the solution. Hence, a correlation exists between the sensor topology and localization accuracy. As shown in Fig. 3, we selected any three of the sensors used for the

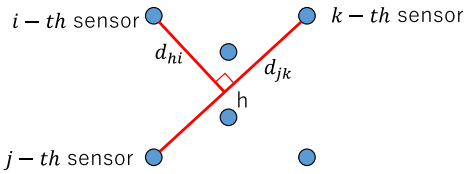

FIGURE 3. Aspect ratio of sensors.

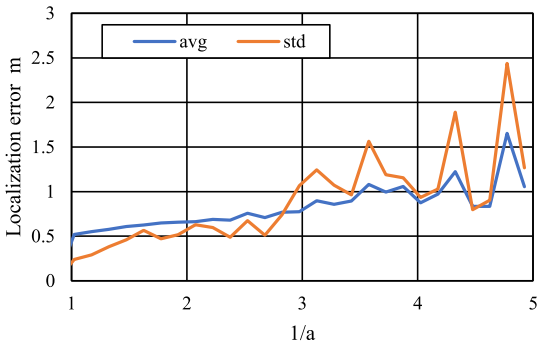

FIGURE 4. Relationship between aspect ratio and localization error.

estimation and labeled them as i-th, j-th, and k-th sensors. The ratio of the line length between j-th and k-th sensors and the length between i-th sensor and $j-k$ line was calculated as the aspect ratio, and this ratio was calculated for all combinations. The maximum value was defined as the aspect ratio of the sensor subset. The resulting value a is given as

$$a = \max_{i\neq j, j\neq k, k\neq i, (i,j,k)=\{1,2,\ldots,N\}} \left\{ \frac{\min\left(d_{hi}, d_{jk}\right)}{\max\left(d_{hi}, d_{jk}\right)} \right\}, \quad (6)$$

where d_{hi} is the distance from the i-th sensor to intersection point h of the $j-k$ vertical line and d_{jk} is the line length of j-th and k-th sensors. The maximum value of a is one, and when it is approximately one, the localization accuracy is recognized as high.

We confirmed the correlation between aspect ratio a and localization accuracy by numerical simulation, as shown in Fig. 4, where the correlation between the localization error and $1/a$, which is the reciprocal of the aspect ratio, is drawn after 100000 localization trials with sensors and targets placed in random positions on a 10 m square plane. The number of sensors was randomly determined to be 3–8, and the channels between the target and sensors were assumed to be in LOS environments. In the legend of Fig. 4, the average and std are the mean and standard deviation of the error results for each $1/a$ grid, respectively. The results show that the mean value is approximately proportional to the value of $1/a$, that is, when a is large, the estimation accuracy tends to be high, but the standard deviation increases. This is because the smaller the aspect ratio, the more biased the sensor positions. Subsequently, the localization results tend to be classified as highly or not highly accurate. However, this study focused on improving the average performance rather than the variance because improving the average was the most effective way of

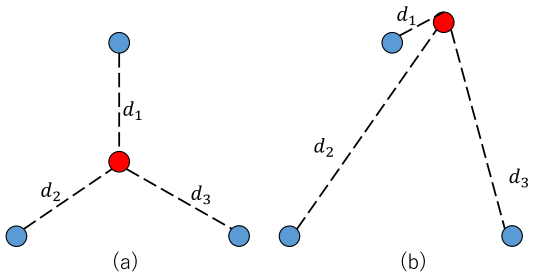

FIGURE 5. Bias of distance between estimated position and sensors.

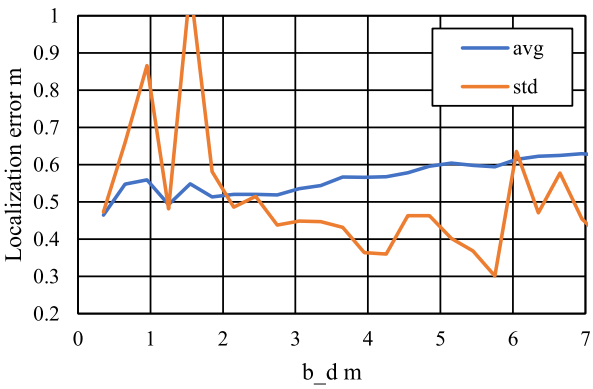

FIGURE 6. Relationship between localization error and bias of distances between estimated position and sensors.

improving the accuracy performance in terms of the root mean square error (RMSE) as defined in (11).

2) DISTANCE BIAS

Localization accuracy is also related to the bias of the distance from the estimated position to each sensor. In general, when the sensors are equidistant from the estimated position, as shown in Fig. 5(a), the localization accuracy becomes high, and when the distance is biased, as shown in (b), the accuracy decreases. This is due to the use of a triangulation algorithm. Based on this, parameter b_d, which predicts the localization accuracy, is defined as

$$b_d = \max_{i\in\{1,2,\ldots,N\}} \{d_i\} - \min_{i\in\{1,2,\ldots,N\}} \{d_i\}, \quad (7)$$

where d_i is the distance between the $i \in \{12, \ldots, N\}$-th sensor and estimated position. b_d is defined not as the variance of d_i but as a difference range [46] of their maximum and minimum values because the number of samples for d_i is insufficient for calculating the variance for small N, such as three or four. We confirmed the b_d by numerical simulations with the same conditions of Fig. 4. The results in Fig. 6 show that although the graphs vary, as shown in Fig. 4, the average of b_d is roughly and inversely proportional to the localization accuracy. Thus, b_d can be used as an indicator of the localization accuracy.

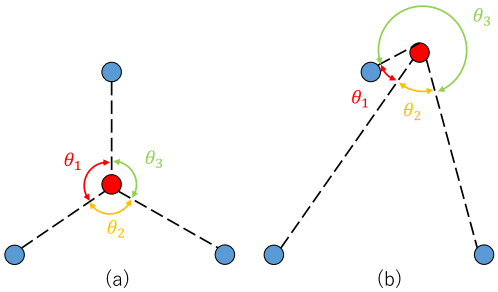

FIGURE 7. Bias of the interior angle formed by the straight line extended from the estimated position to the sensors.

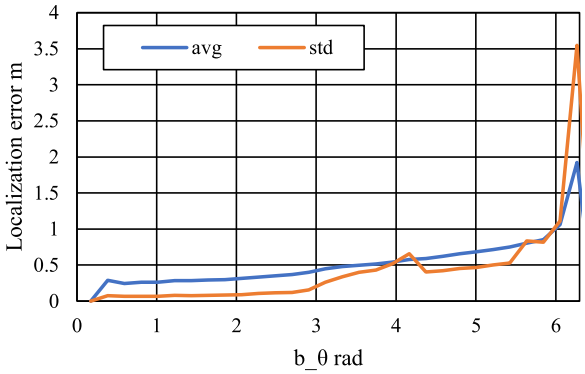

FIGURE 8. Relationship between interior angle bias and localization accuracy.

3) ANGLE BIAS

A relationship exists between the localization accuracy and bias of the angle formed by the straight lines from the estimated position to each sensor. As shown in Fig. 7, the localization accuracy is expected to be high in the case of (a) by balanced topology, whereas it is expected to be low in the case of (b) owing to the biased topology. From this perspective, the parameter b_θ, which is inversely proportional to the localization accuracy, is defined as

$$b_\theta = \max_{l\in\{1,2,\ldots,N\}} \{\theta_l\} - \min_{l\in\{1,2,\ldots,N\}} \{\theta_l\}, \tag{8}$$

where θ_l is the l-th angle among N internal angles from the estimated position to the two adjacent sensors. The correlation between b_θ and localization accuracy was examined in the same manner as for a and b_d. The results are shown in Fig. 8. The localization accuracy can be observed to be greatly degraded in region of $b_\theta > 6.0$ rad along the horizontal axis. However, this indicates an existence of an angular bias of approximately 360°, which is considered an extremely rare case in the practical sensor field. Therefore, b_θ was confirmed to be approximately proportional to the localization error in the region of $b_\theta \leq 6.0$ rad. Hence, b_θ is concluded to be inversely proportional to the localization accuracy.

Because each of these variables a, b_d, and b_θ can take an independent value, we define the overall reliability index

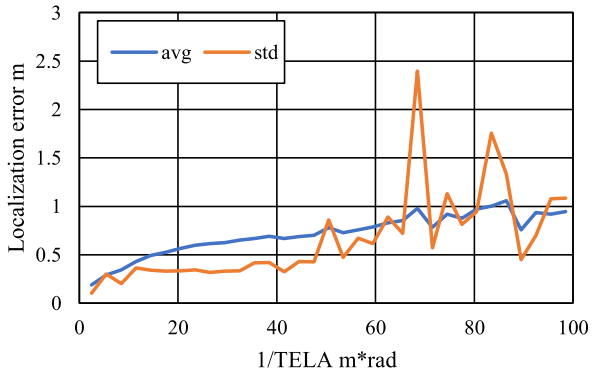

FIGURE 9. Relationship between TELA and localization error.

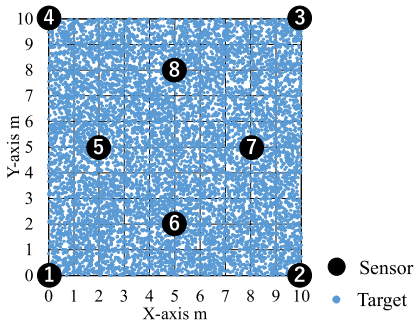

FIGURE 10. Sensor field in numerical simulation.

TELA using all variables as

$$t_j = \frac{a}{b_d b_\theta}, \tag{9}$$

where t_j denotes the TELA value at j-th estimated position. The correlation between TELA and localization accuracy was also confirmed by numerical simulations, as shown in Fig. 9. This indicates that the localization error increased as the value of 1/TELA increased, that is, the higher the value of TELA, the higher the localization accuracy.

Considering the characteristics of t_j, the final estimated position $\mathbf{z} = (\bar{x}, \bar{y})$ can be obtained by the weighted average of the estimated positions using TELA, as follows:

$$\mathbf{z} = \frac{\sum_{j\in M_{LOS}} t_j \mathbf{z}_j}{\sum_{j\in M_{LOS}} t_j}, \tag{10}$$

where $\mathbf{z}_j$ denotes the j-th estimated position.

IV. NUMERICAL RESULTS

The performance of the proposed method was evaluated using numerical simulations. Fig. 10 shows the sensor field in which eight sensors were deployed. NLOS sensors were assumed to exist randomly from zero to four of the eight sensors in every trial. The position of the target sensor was also random in each trial. The simulation conditions are listed in Table 1. In conventional methods, the performances of location-based LS [41], LMedS [28], IMR [34], and NEMIRC [35] methods are plotted. The LS method is the basic multilateration estimation method, and the LLS is used to minimize the squared sum

TABLE 1 Simulation Conditions

Localization method	LS, IMR, LMedS, NEMIRC, proposed method
Sensor field	10 m × 10 m
Number of sensor nodes N	8
Target node position	random
Distribution of NLOS sensors	random
Ranging method	Average of 30 measurements
Number of simulation trials n_{loop}	10,000
Threshold of residual δ	0.3 m^2
Reliability threshold of distance measurement value τ	0.0 m
UWB bandwidth	500 MHz
Parameters of TOA-LOS error	$\mu_{\mathrm{LOS}} = 0.21$ m $\sigma^2_{\mathrm{LOS}} = 0.269^2$ m^2
Parameters of TOA-NLOS error	$\mu_{\mathrm{NLOS}} = 1.62$ m $\sigma^2_{\mathrm{NLOS}} = 0.809^2$ m^2

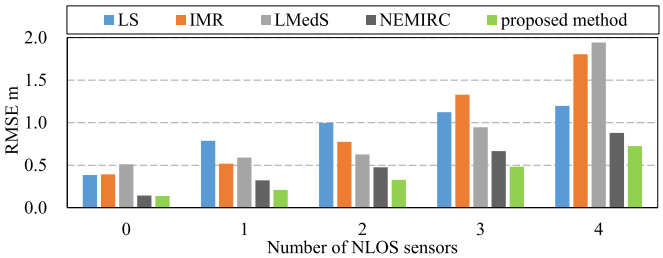

FIGURE 11. RMSE performance comparison when all eight sensors are used.

of the residual error. Similarly, LS is used in the localization of IMR, LMedS, NEMIRC, and the proposed methods. The performance was evaluated by the RMSE, which is given by

$$RMSE = \sqrt{\sum_{n=1}^{n_{loop}} \frac{\left(x_{\mathrm{tag}} - \hat{x}_n\right)^2 + \left(y_{\mathrm{tag}} - \hat{y}_n\right)^2}{n_{loop}}} \tag{11}$$

Here, $(x_{\mathrm{tag}}, y_{\mathrm{tag}})$ and $(\hat{x}_n, \hat{y}_n)$ are the true position of the target and estimated position at the n-th trial, respectively, and n_{loop} is the number of trials. Note that TELA only measures the topological heterogeneity of the sensor nodes, which only indirectly contributes to the final required performance, that is, the mean squared error improvement. The final accuracy evaluation was performed using RMSE. The distance and TOA propagation model were assumed to be given by the following equation and as listed in Table 1 [45]:

$$\begin{aligned} \hat{d} &= d + n_{\mathrm{LOS}} + \zeta n_{\mathrm{NLOS}} \\ n_{\mathrm{LOS}} &\sim N\left(\mu_{\mathrm{LOS}} \log\left(1.0 + d\right), \sigma^2_{\mathrm{LOS}}\left[\log\left(1.0 + d\right)\right]^2\right) \\ n_{\mathrm{NLOS}} &\sim N\left(\mu_{\mathrm{NLOS}}, \sigma^2_{\mathrm{NLOS}}\right), \end{aligned} \tag{12}$$

where d is the true distance between the target and sensor, and ζ is a switching parameter equal to zero in the LOS environment and one in the NLOS environment.

Fig. 11 shows the RMSE performance versus the number of NLOS environmental sensors when using all eight sensors.

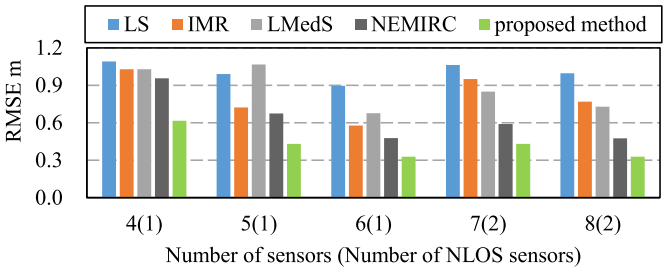

FIGURE 12. RMSE performance when the number of sensors is varied.

The proposed method can be observed to exhibit the smallest RMSE in all cases, indicating accurate localization. The conventional method uses either the residuals or reliability of ranging values for NLOS discrimination for improving localization accuracy. In contrast, the proposed method uses both of these and improves the accuracy of NLOS discrimination. The TELA weighted average of estimated locations employed more weights for reliable estimated locations and improved the RMSE in both LOS and NLOS environments. This is the novelty of the proposed method. However, we found that when half of the sensors (e.g., four out of eight sensors) were NLOS sensors, the RMSE of the proposed method increased, similar to the NEMIRC method. This can be regarded as a limitation of our proposed method.

Fig. 12 shows the RMSE performance when the numbers of total sensors N and NLOS sensors are varied from four to eight and from one to two, respectively, as shown in Fig. 10. For each N, sensors labeled from 1 to N were used and the NLOS sensors were randomly placed. On the horizontal axis of Fig. 12, for example, 6(1) indicates one sensor in an NLOS environment among $N = 6$ sensors. The results confirm the superiority of the proposed method in all the cases. In particular, when the number of sensors was four, the proposed method exhibited a significant improvement compared with the other methods. This is because the weight of TELA works effectively in an environment with less number of sensors, where the performance degradation by an NLOS sensor is relatively large.

Next, we examined the impact of each TELA factor on the localization accuracy. The simulation was performed 100000 times with the number of NLOS sensors set to 1 in the sensor field, as shown in Fig. 10. Fig. 13 shows the results, which indicate that each element of TELA contributed to improved localization accuracy. Each of these elements is individually effective and they are even more effective when combined and used as TELA.

Table 2 shows the improvement percentage of the proposed method compared to the state-of-the-art NEMIRC method. An improvement of 37% can be observed at maximum in the proposed method over the conventional method.

Finally, we evaluated the method for specific scenarios. We considered two scenarios in the sensor field, as shown in Fig. 14. Scenario (1) assumed the target position set to (37) and sensor No. 6 in an NLOS environment. In scenario (2),

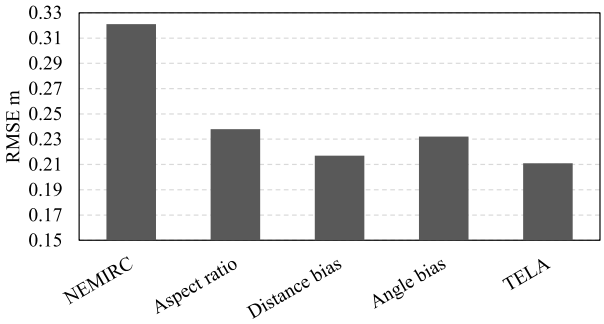

FIGURE 13. Impact of each element of TELA for localization accuracy. Sensor field is equal to that in Fig. 10 and the number of NLOS sensors is one.

TABLE 2 Improvement Percentage of Proposed Method Over NEMIRC Method

No. of NLOS sensors (Fig. 11)	0	1	2	3	4
Improvement %	4.13	34.76	33.33	27.32	17.66
No. of sensors (NLOS) (Fig. 12)	4(1)	5(1)	6(1)	7(2)	8(2)
Improvement %	36.84	36.76	28.89	24.14	28.89

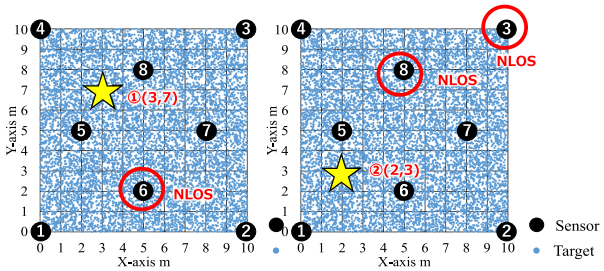

FIGURE 14. Specific simulation scenarios. Sensor field is the same as in Fig. 10 with fixed target location and NLOS environmental sensors.

TABLE 3 Performance Comparison at Specific Location

	Scenario 1	Scenario 2
Target true location	(3,7)	(2,3)
Estimated location with LS	(2.690,7.579)	(0.879,1.368)
Estimated location with NEMIRC	(2.813,7.046)	(1.878,2.943)
Estimated location with TELA	(2.918,7.047)	(1.920,3.036)
RMSE with LS	0.657 m	1.98 m
RMSE with NEMIRC	0.193 m	0.135 m
RMSE with TELA	0.094 m	0.088 m

the target position was set to (23) and sensors 3 and 8 were in the NLOS environment. The simulation results using the same ranging noise model as in Figs. 11 and 12 are shown in Table 3. The proposed method can be observed to exhibit the highest localization accuracy.

V. CALCULATION COMPLEXITY ANALYSIS AND THEORETICAL LOWER BOUND OF LOCALIZATION ACCURACY

Because the proposed method, like the conventional methods of IMR and LMedS, does not require any prior information, such as channel state information, it is categorized as low-complexity localization and is suitable for real-time tracking. Therefore, the low-complexity property is important in the proposed method. This section investigates the calculation complexity and performance bounds for the proposed and conventional methods, and evaluates their practicality.

TABLE 4 Comparison of Required Calculation Complexity

Algorithm	Numerical cost
LS	$O(N)$
IMR	$O(N^3)$
LMedS	$O(N^5)$
NEMIRC	$O(N2^{N-1})$
Proposed method	$O(N2^{N-1})$

A. CALCULATION COMPLEXITY

We used the widely used Landau symbol O [46] as the complexity indicator. Table 4 lists the order of complexity of each method, where N is the number of sensor nodes. The proposed method can be observed to exhibit the highest complexity. However, if the number of sensors is 10, the order becomes $O(10 \times 2^9)$, which can be easily calculated using a current-model desktop computer. The derivations in Table 4 are as follows:

First, the LS method is equivalent to solving N simultaneous equations in which the unknown parameters are the coordinates $(x,\ y)$ and the order becomes $O(N)$.

Second, in the IMR method, the sequential elimination of NLOS sensors contributes to dominant complexity. This operation is conducted one by one for each sensor until the number of residual sensors is at a maximum, and then the complexity becomes

$$O\left(\sum_{n=4}^{N} n\,(n-1)\right) = O\left(N^3\right) \tag{13}$$

The LMedS method iteratively estimated the position with all subsets of the three sensors and selected the best subset with the lowest center value of residual error. The number of subsets is

$$\binom{N}{3} = \frac{N\,(N-1)\,(N-2)}{6} = \frac{1}{6}\left(N^3 - 3N^2 + 2N\right) \tag{14}$$

In each subset, localization and sorting were performed for selecting the central value. Then, the complexity becomes

$$O\left(\frac{1}{6}\left(N^3 - 3N^2 + 2N\right)\right) \times O\left(N^2\right) = O\left(N^5\right) \tag{15}$$

Finally, the calculation complexity of the NEMIRC and proposed method was considered. Calculation complexity becomes the largest when all the sensor combinations are explored in an LOS environment. The number of combinations of all sensors is M can be calculated from (1). For each combination of k sensors, the distance $\hat{d}_i$ for localization was measured, and the LLS localization of (2) and reliability evaluation of (4) were conducted. In addition, the TELA calculation given by (9) was performed only in the proposed method. Because all these calculation complexities were $O(k)$, the maximum calculation complexity converged

TABLE 5 Comparison of Calculation Complexity at $N = 10$

Algorithm	Normalized complexity at $N =$ 10 when LS method is 1
LS	1
IMR	52
LMedS	120
NEMIRC	968
Proposed method	968

to $O(k)$. Therefore, the calculation complexity of the entire algorithm becomes

$$O\left(\sum_{k=3}^{N}\binom{N}{k}k\right) = O\left(N2^{N-1}\right) \tag{16}$$

After all sensor combinations were explored in the LOS environment, the calculation complexity of NEMIRC and proposed method attained a maximum value. However, as the number of NLOS sensors increased, the number of sensor combinations not considered after (4) increased and the calculation complexity decreased.

In addition, specific numerical calculations were performed for better understanding. Assuming $N = 10$, we compared the number of times the LS position estimation was performed between the conventional and proposed algorithms. Table 5 summarizes the normalized calculation complexities using the LS method. The results show that the LS method was iterated 968 times using the proposed method. Because the computational complexity exponentially increases as N increases, devising a distributed implementation algorithm, such as separating sensor fields for large N, may be necessary.

B. PERFORMANCE OF CRAMER-RAO LOWER BOUND

An unbiased estimator that estimates the unknown parameters of a certain probability distribution has a lower bound on variance. This is called the CRLB [47], [48], [49], [50] and is widely used to evaluate the effectiveness of estimations, such as localization. We assumed $d_i(\boldsymbol{\varphi}_t)$ to be the true distance between the i-th sensor node of $i = 12, \ldots, N$ and target of the coordinate $\boldsymbol{\varphi}_t = (x_t, y_t)$ and is given using the sensor coordinate (x_i, y_i) as

$$d_i\left(\boldsymbol{\varphi}_t\right) = \sqrt{(x_t - x_i)^2 + (y_t - y_i)^2} \tag{17}$$

When the measurement error of the measured distance $\hat{d}_i$ is stochastically independent and subject to the same distribution, the likelihood function $l(\boldsymbol{\varphi})$ of coordinate $\boldsymbol{\varphi} = (x, y)$ with the measured distance $\hat{d}_i$ is given by

$$l\left(\boldsymbol{\varphi}\right) = p\left(\hat{d}_1, \ldots, \hat{d}_i, \ldots, \hat{d}_N|\boldsymbol{\varphi}\right) = \prod_{i=1}^{N} p\left(\hat{d}_i|\boldsymbol{\varphi}\right) \tag{18}$$

Then, localization was performed by obtaining $\boldsymbol{\varphi}$ that maximizes (18). By taking logarithm of (18),

$$\begin{aligned} L\left(\boldsymbol{\varphi}\right) &= \sum_{i=1}^{N} \log p\left(\mathbf{D}_i|\boldsymbol{\varphi}\right), \\ &= \sum_{l=1}^{L}\sum_{i=1}^{N} \log p\left(\hat{d}_{il}|d_i\left(\boldsymbol{\varphi}\right)\right), \\ &= \sum_{i=1}^{N} L \log p\left(\hat{d}_i|d_i\left(\boldsymbol{\varphi}\right)\right) = \sum_{i=1}^{N} L_i\left(\boldsymbol{\varphi}\right), \end{aligned} \tag{19}$$

where $\mathbf{D}_i = \{\hat{d}_{i1}, \hat{d}_{i2}, \ldots, \hat{d}_{iL}\}$ is the vector of the measured distance values of the i-th sensor; L is the number of distance measurements at each sensor; $L_i(\boldsymbol{\varphi}) = \log p(\mathbf{D}_i|\boldsymbol{\varphi})$, $l(= 1, \ldots, L)$ is the index of the measurement data; $\hat{d}_{il}$ is the measured distance of the i-th sensor at the l-th measurement; and the measurement errors are assumed to obey the same distribution. The CRLB can be calculated from the Fisher information matrix (FIM) [48], and the FIM of (19) is given by

$$J_F\left(\boldsymbol{\varphi}\right) = -\mathrm{E}\begin{bmatrix} \frac{\partial^2}{\partial x^2}L\left(\boldsymbol{\varphi}\right) & \frac{\partial^2}{\partial x \partial y}L\left(\boldsymbol{\varphi}\right) \\ \frac{\partial^2}{\partial x \partial y}L\left(\boldsymbol{\varphi}\right) & \frac{\partial^2}{\partial y^2}L\left(\boldsymbol{\varphi}\right) \end{bmatrix} = \begin{bmatrix} J_{11} & J_{12} \\ J_{21} & J_{22} \end{bmatrix}, \tag{20}$$

where E[] denotes the stochastic average. Each element of (20) is given by

$$\begin{aligned} J_{11} &= -\mathrm{E}\left[\frac{\partial^2}{\partial x^2}L\left(\boldsymbol{\varphi}\right)\right], \\ &= -L\sum_{i=1}^{N}\xi_i\left(\boldsymbol{\varphi}\right)\left(\frac{\partial d_i\left(\boldsymbol{\varphi}\right)}{\partial x}\right)^2, \end{aligned} \tag{21}$$

where

$$\xi_i\left(\boldsymbol{\varphi}\right) = \mathrm{E}\left[\frac{\partial L_n\left(\boldsymbol{\varphi}\right)}{\partial d_i(\boldsymbol{\varphi})^2}\right] \tag{22}$$

In the same way, J_{22}, J_{12}, and J_{21} are obtained by

$$J_{22} = -L\sum_{i=1}^{N}\xi_i\left(\boldsymbol{\varphi}\right)\left(\frac{\partial d_i\left(\boldsymbol{\varphi}\right)}{\partial y}\right)^2, \tag{23}$$

$$J_{12} = J_{21} = -L\sum_{i=1}^{N}\xi_i\left(\boldsymbol{\varphi}\right)\frac{\partial d_i\left(\boldsymbol{\varphi}\right)}{\partial x}\frac{\partial d_i\left(\boldsymbol{\varphi}\right)}{\partial y}, \tag{24}$$

where the inverse matrix of FIM can be defined by

$$\begin{aligned} I_F\left(\boldsymbol{\varphi}\right) &= J_F^{-1}\left(\boldsymbol{\varphi}\right) \\ &= \begin{bmatrix} I_{11} & I_{12} \\ I_{21} & I_{22} \end{bmatrix} \\ &= \frac{1}{J_{11}J_{22} - J_{12}J_{21}}\begin{bmatrix} J_{22} & -J_{12} \\ -J_{21} & J_{11} \end{bmatrix} \end{aligned} \tag{25}$$

Then, the lower bound of the estimation error variance in the maximum likelihood estimation can be calculated as

$$\begin{aligned} &\sigma^2_{CRLB}\left(\boldsymbol{\varphi}\right) \\ &= \min\left\{\mathrm{var}\left(x\right) + \mathrm{var}\left(\mathrm{y}\right)\right\} = I_{11} + I_{22} = \frac{J_{22} + J_{11}}{J_{11}J_{22} - J_{12}J_{21}} \\ &= \left\{-\sum_{i=1}^{N}\xi_i\left(\boldsymbol{\varphi}\right)\left(\frac{x - x_i}{d_i\left(\boldsymbol{\varphi}\right)}\right)^2 - \sum_{i=1}^{N}\xi_i\left(\boldsymbol{\varphi}\right)\left(\frac{y - y_i}{d_i\left(\boldsymbol{\varphi}\right)}\right)^2\right\} \end{aligned}$$

$$\times \left[L \left\{ \sum_{i=1}^{N} \xi_i(\boldsymbol{\varphi}) \left(\frac{x - x_i}{d_i(\boldsymbol{\varphi})} \right)^2 \right\} \left\{ \sum_{i=1}^{N} \xi_i(\boldsymbol{\varphi}) \left(\frac{y - y_i}{d_i(\boldsymbol{\varphi})} \right)^2 \right\} - L \left\{ \sum_{i=1}^{N} \xi_i(\boldsymbol{\varphi}) \left(\frac{x - x_i}{d_i(\boldsymbol{\varphi})} \right) \left(\frac{y - y_i}{d_i(\boldsymbol{\varphi})} \right) \right\}^2 \right]^{-1}, \tag{26}$$

where var() denotes the variance. For calculating (26), the measurement noise model is required. In conventional studies, a channel model that does not consider wireless distance [49] and other models that consider path loss [48], [50] have been proposed. However, the CRLB of the channel model [45] assumed in this study was not studied, and has thus been derived as follows; The noise model in the LOS environment in [45] is given by

$$p_{\mathrm{LOS}}\left(\hat{d}_i | d_i(\boldsymbol{\varphi})\right) = \frac{1}{\sqrt{2\pi}\sigma_{\mathrm{LOS}} S_{\mathrm{LOS}}} \exp\left[-\frac{\left(\hat{d}_i - d_i(\boldsymbol{\varphi}) - \mu_{\mathrm{LOS}} S_{\mathrm{LOS}}\right)^2}{2(\sigma_{\mathrm{LOS}} S_{\mathrm{LOS}})^2} \right], \tag{27}$$

where

$$S_{\mathrm{LOS}} = \log\left(1 + d_i(\boldsymbol{\varphi})\right) \tag{28}$$

Here, μ_{LOS} and σ_{LOS} are the LOS environmental parameters mean and variance, respectively. In this case, the parameter $\xi_i(\boldsymbol{\varphi})$ in (27) is calculated as

$$\xi_i(\boldsymbol{\varphi}) = \frac{1}{(1 + d_i(\boldsymbol{\varphi}))^2} + \frac{1}{\sigma_{\mathrm{LOS}}^2} \left\{ -\frac{(1 + d_i(\boldsymbol{\varphi}) + \mu_{\mathrm{LOS}})^2}{S_{\mathrm{LOS}}^2 (1 + d_i(\boldsymbol{\varphi}))^2} - \frac{3 + S_{\mathrm{LOS}}}{S_{\mathrm{LOS}}^4 (1 + d_i(\boldsymbol{\varphi}))^2} \left((\sigma_{\mathrm{LOS}} S_{\mathrm{LOS}})^2 - (d_i(\boldsymbol{\varphi}))^2 \right) \right\} \tag{29}$$

as shown in Appendix B. The CRLB of the LOS environment can then be obtained by substituting (29) into (26):

Similarly, in the NLOS case, the noise model [47] is given by

$$p_{\mathrm{NLOS}}\left(\hat{d}_i | d_i(\boldsymbol{\varphi})\right) = \frac{1}{\sqrt{2\pi}\mathrm{S}_{\mathrm{NLOS}}} \times \exp\left[-\frac{\left(\hat{d}_i - d_i(\boldsymbol{\varphi}) - \mu_{\mathrm{LOS}} \log(1 + d_i(\boldsymbol{\varphi})) - \mu_{\mathrm{NLOS}}\right)^2}{2\mathrm{S}_{\mathrm{NLOS}}} \right], \tag{30}$$

here

$$p_{\mathrm{NLOS}}\left(\hat{d}_i | d_i(\boldsymbol{\varphi})\right) = \frac{1}{\sqrt{2\pi}\mathrm{S}_{\mathrm{NLOS}}} \times \exp\left[-\frac{\left(\hat{d}_i - d_i(\boldsymbol{\varphi}) - \mu_{\mathrm{LOS}} \log(1 + d_i(\boldsymbol{\varphi})) - \mu_{\mathrm{NLOS}}\right)^2}{2\mathrm{S}_{\mathrm{NLOS}}} \right] \tag{31}$$

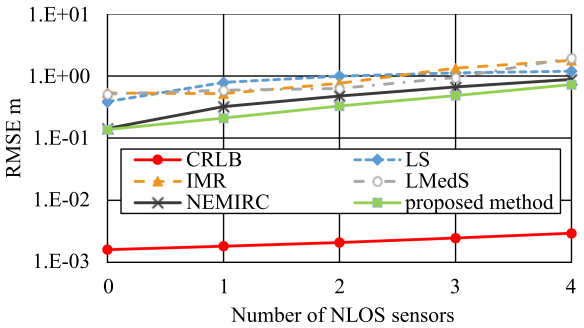

FIGURE 15. Comparison of RMSE performance to Cramer–Rao lower bound.

Subsequently, $\xi_i(\boldsymbol{\varphi})$ can be obtained as

$$\xi_i(\boldsymbol{\varphi}) = \frac{\sigma_{\mathrm{LOS}}^2 \log(1 + d_i(\boldsymbol{\varphi})) - (1 + d_i(\boldsymbol{\varphi}) + \mu_{\mathrm{LOS}})^2}{S_{\mathrm{NLOS}}(1 + d_i(\boldsymbol{\varphi}))^2} + \frac{\sigma_{\mathrm{LOS}}^2 \left\{ 2\left(\sigma_{\mathrm{LOS}} \log(1 + d_i(\boldsymbol{\varphi}))\right)^2 - d_i(\boldsymbol{\varphi}) \right\}}{S_{\mathrm{NLOS}}^2 (1 + d_i(\boldsymbol{\varphi}))^2} + \{S_{\mathrm{NLOS}} - d_i(\boldsymbol{\varphi})\} \frac{\sigma_{\mathrm{LOS}}^2 \log(1 + d_i(\boldsymbol{\varphi})) \{4\sigma_{\mathrm{LOS}}^2 \log(1 + d_i(\boldsymbol{\varphi})) + S_{\mathrm{NLOS}}^2\}}{S_{\mathrm{NLOS}}^3 (1 + d_i(\boldsymbol{\varphi}))^2} \tag{32}$$

as shown in Appendix C. The CRLB of the NLOS environment was obtained by substituting (32) into (26). Using these results, the RMSE performances of the conventional and proposed methods were compared to those of the CRLB, in which the simulation conditions were the same as those in Section IV and Table 1. The results in Fig. 15 show that the CRLB was much lower than the other methods because the conventional and proposed methods are location-based algorithms that do not use any prior information, whereas CRLB assumes that the noise model is known. Fig. 15 also shows that the proposed method exhibits the best performance compared with the CRLB. In conclusion, the proposed method is the closest to CRLB, is a practical method that does not require prior information, and is suitable for real-time applications.

VI. EXPERIMENTAL RESULTS

We evaluated the performance of the proposed method through experiments performed at the National Institute of Information and Communications Technology in the Yokosuka Research Park. A real-time location system (RTLS) based on the UWB RTLS Starter Kit from GIT Inc. [51] was used in our experiment (Fig. 16). Fig. 17 shows the experimental room layout, where five sensors were deployed in a 15.5 m × 9.0 m room with the origin at the lower left side. The rooms were constructed for office use and had plaster ceilings and carpeting, concrete walls, and steel room partitions. Glass windows also existed. The NLOS environment was simulated by shielding direct waves between the sensors and target with metal plates, and verification was carried out using one and two NLOS environmental sensors, called Scenarios 1 and 2, respectively.

FIGURE 16. UWB RTLS Starter Kit from GIT used in the experiment.

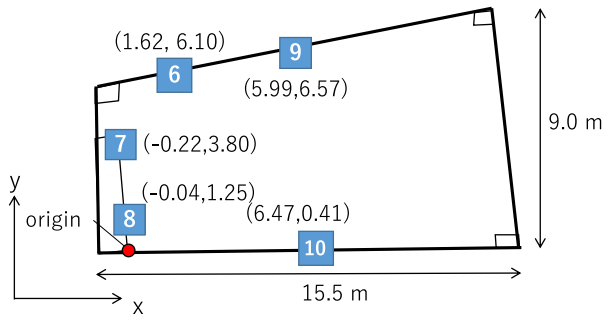

FIGURE 17. Room layout and experimental settings.

TABLE 6 Specifications of Experiments

Scenario	Scenario 1	Scenario 2
Sensor numbers	#6, #7, #8, #9, #10	
NLOS node(s)	#6	#6, #7
True position of the target in m	(5.20, 3.07)	(5.29, 2.82)
Ranging method	Average of the 30 measurements	
Residual threshold	0.5 m^2	
Means of NLOS environment	Blockage by metal plates	
Number of experiments	10	
Model number of UWB sensor	UWB RTLS Starter Kit	
Bandwidth	3 GHz (7.25-10.25 GHz)	
Average PSD (power spectrum density)	$-41.3\ dBm/\text{MHz}$	
Peak PSD (power spectrum density)	$0\ dBm/50$ MHz	
Pulse rate	50 Mpps	

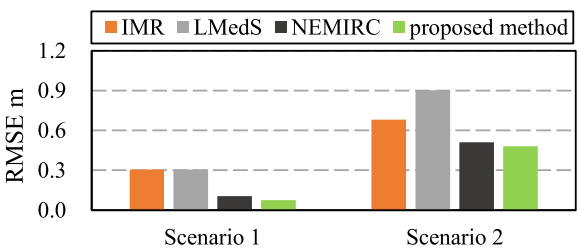

FIGURE 18. Experimental result of RMSE.

The experimental conditions and main specifications of the UWB RTLS are listed in Table 6. Notably, the UWB RTLS system is certified for license-exempt operations.

Fig. 18 shows the performance of RMSE. The experimental results verified the effectiveness of the proposed method. As shown in the numerical results, the weighted summation of the estimated positions by TELA were observed to achieve a higher localization accuracy than conventional methods.

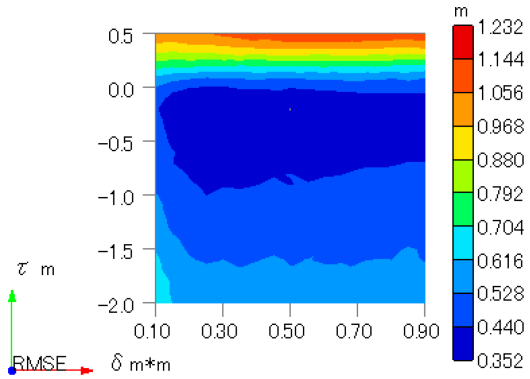

FIGURE 19. Determination of optimal thresholds δ and τ for proposed method.

VII. CONCLUSION

In this paper, we proposed a new location-based method for accurate localization using NLOS environmental sensor elimination, which does not require any prior information. In conventional methods, either residual errors or reliability of the ranging value are used for NLOS sensor detection, and detection errors often occur in many NLOS sensor cases. In the proposed method, we improved the accuracy of NLOS detection using both the methods. Furthermore, the newly proposed TELA was adopted for the estimated positions of various sensor combinations as a weighted summation to realize accurate localization in both LOS and NLOS environments. Numerical results revealed its superior performance, and by analyzing the calculation complexity and CRLB, the proposed method was shown to exhibit high practicability in terms of performance and calculation complexity. Furthermore, the effectiveness of the proposed method was experimentally confirmed.

APPENDIX

A. DETERMINATION OF OPTIMAL THRESHOLDS δ AND τ FOR PROPOSED METHOD

The proposed method requires thresholds δ for the residuals and τ for the reliability of the ranging values to extract the estimated positions determined only in the LOS environment. Here, we numerically derive the optimal values. The numerical simulation was performed under the same conditions using eight sensors, as described in Section III. The number of NLOS sensors was changed randomly from zero to four in 10000 simulation trials. The RMSE performance of the proposed method, when the thresholds δ and τ were varied, is shown in Fig. 19, where the horizontal and vertical axes are δ and τ, respectively, and the color indicates the RMSE. The closer the color to blue, the lower the RMSE. The results showed that the performance of the proposed method was stable in the range of $-0.75\ \text{m} \leq \tau \leq 0.0\ \text{m}$ and did not depend much on the threshold of residuals δ. We can eliminate many NLOS environmental estimated positions by setting a

strict threshold, which results in a reduction in the calculation complexity. Therefore, we set $\delta = 0.3$ m^2 and $\tau = 0.0$ m in this paper.

B. DERIVATION OF $\xi_i(\varphi)$ IN LOS ENVIRONMENTS

In LOS environments, the measurement noise obeys the probability of (27), and thus

$$\begin{aligned}
&\xi_i(\boldsymbol{\varphi}) \\
&= \mathrm{E}\left[\frac{\partial^2}{\partial d_i(\boldsymbol{\varphi})^2}\log\left\{\frac{1}{\sqrt{2\pi}\sigma_{\mathrm{LOS}}S_{\mathrm{LOS}}}\exp\left[-\frac{R_{\mathrm{LOS}}^2}{2\{\sigma_{\mathrm{LOS}}S_{\mathrm{LOS}}\}^2}\right]\right\}\right] \\
&= \mathrm{E}\left[\frac{1}{\left(1+d_i(\boldsymbol{\varphi})^2\right)^2} + \frac{1}{\sigma_{\mathrm{LOS}}^2}\left\{-\frac{\left(1+d_i(\boldsymbol{\varphi})^2+\mu_{\mathrm{LOS}}\right)^2}{S_{\mathrm{LOS}}^2\left(1+d_i(\boldsymbol{\varphi})^2\right)^2}\right.\right. \\
&\quad -\left\{\frac{\mu_{\mathrm{LOS}}}{S_{\mathrm{LOS}}^2\left(1+d_i(\boldsymbol{\varphi})^2\right)^2} + \frac{4\left(1+d_i(\boldsymbol{\varphi})^2+\mu_{\mathrm{LOS}}\right)}{S_{\mathrm{LOS}}^3\left(1+d_i(\boldsymbol{\varphi})^2\right)^2}\right\}R_{\mathrm{LOS}} \\
&\quad \left.\left.-\frac{3+S_{\mathrm{LOS}}}{S_{\mathrm{LOS}}^4\left(1+d_i(\boldsymbol{\varphi})^2\right)^2}R_{\mathrm{LOS}}^2\right\}\right] \qquad (33)
\end{aligned}$$

is obtained, where

$$R_{\mathrm{LOS}} = \hat{d}_i - d_i(\boldsymbol{\varphi}) - \mu_{\mathrm{LOS}}\log\left(1+d_i(\boldsymbol{\varphi})\right) \qquad (34)$$

Here, using the stochastic nature, the following equations hold:

$$\mathrm{E}\left[\hat{d}_i\right] = d_i(\boldsymbol{\varphi}) + \mu_{\mathrm{LOS}}\log\left(1+d_i(\boldsymbol{\varphi})\right) \qquad (35)$$

$$\mathrm{E}\left[\left(\hat{d}_i - \mu_{\mathrm{LOS}}\log\left(1+d_i(\boldsymbol{\varphi})\right)\right)^2\right] = \left(\sigma_{\mathrm{LOS}}\log\left(1+d_i(\boldsymbol{\varphi})\right)\right)^2 \qquad (36)$$

$$\mathrm{E}\left[\hat{d}_i - \mu_{\mathrm{LOS}}\log\left(1+d_i(\boldsymbol{\varphi})\right)\right] = d_i(\boldsymbol{\varphi}) \qquad (37)$$

Therefore,

$$\mathrm{E}\left[R_{\mathrm{LOS}}\right] = 0 \qquad (38)$$

$$\mathrm{E}\left[R_{\mathrm{LOS}}^2\right] = \left(\sigma_{\mathrm{LOS}}\log\left(1+d_i(\boldsymbol{\varphi})\right)\right)^2 - \left(d_i(\boldsymbol{\varphi})\right)^2 \qquad (39)$$

are given and (33) becomes

$$\begin{aligned}
\xi_i(\boldsymbol{\varphi}) &= \frac{1}{\left(1+d_i(\boldsymbol{\varphi})\right)^2} \\
&\quad + \frac{1}{\sigma_{\mathrm{LOS}}^2}\left\{-\frac{\left(1+d_i(\boldsymbol{\varphi})+\mu_{\mathrm{LOS}}\right)^2}{S_{\mathrm{LOS}}^2\left(1+d_i(\boldsymbol{\varphi})\right)^2}\right. \\
&\quad \left.-\frac{3+S_{\mathrm{LOS}}}{S_{\mathrm{LOS}}^4\left(1+d_i(\boldsymbol{\varphi})\right)^2}\left(\left(\sigma_{\mathrm{LOS}}S_{\mathrm{LOS}}\right)^2 - \left(d_i(\boldsymbol{\varphi})\right)^2\right)\right\}
\end{aligned} \qquad (40)$$

C. DERIVATION OF $\xi_i(\varphi)$ IN LOS ENVIRONMENTS

As in Appendix B, in NLOS environments, the measurement noise obeys the probability of (30).

$$\begin{aligned}
\xi_i(\boldsymbol{\varphi}) &= \mathrm{E}\left[\frac{\partial^2}{\partial d_i(\boldsymbol{\varphi})^2}\log\left\{\frac{1}{\sqrt{2\pi S_{\mathrm{NLOS}}}}\exp\left[-\frac{R_{\mathrm{NLOS}}^2}{2S_{\mathrm{NLOS}}}\right]\right\}\right] \\
&= \mathrm{E}\left[-\sigma_{\mathrm{LOS}}^2\frac{S_{\mathrm{NLOS}}-\log(1+d_i(\boldsymbol{\varphi}))\left\{2\sigma_{\mathrm{LOS}}^2\log(1+d_i(\boldsymbol{\varphi}))+S_{\mathrm{NLOS}}\right\}}{S_{\mathrm{NLOS}}^2(1+d_i(\boldsymbol{\varphi}))^2}\right. \\
&\quad -\frac{\left(1+d_i(\boldsymbol{\varphi})+\mu_{\mathrm{LOS}}\right)^2}{S_{\mathrm{NLOS}}\left(1+d_i(\boldsymbol{\varphi})\right)^2} + R_{\mathrm{NLOS}}\left\{\frac{1}{S_{\mathrm{NLOS}}(1+d_i(\boldsymbol{\varphi}))}\right. \\
&\quad -\frac{(1+d_i(\boldsymbol{\varphi})+\mu_{\mathrm{LOS}})\left(2\sigma_{\mathrm{LOS}}^2\log(1+d_i(\boldsymbol{\varphi}))+S_{\mathrm{NLOS}}\right)}{S_{\mathrm{NLOS}}^2(1+d_i(\boldsymbol{\varphi}))^2} \\
&\quad + R_{\mathrm{NLOS}}^2\left\{\frac{\sigma_{\mathrm{LOS}}^2}{S_{\mathrm{NLOS}}^2(1+d_i(\boldsymbol{\varphi}))^2}\right. \\
&\quad \left.\left.\left.+\frac{\sigma_{\mathrm{LOS}}^2\log(1+d_i(\boldsymbol{\varphi}))\left\{4\sigma_{\mathrm{LOS}}^2\log(1+d_i(\boldsymbol{\varphi}))+S_{\mathrm{NLOS}}^2\right\}}{S_{\mathrm{NLOS}}^3(1+d_i(\boldsymbol{\varphi}))^2}\right\}\right\}\right]
\end{aligned} \qquad (41)$$

is obtained, where

$$R_{\mathrm{NLOS}} = \hat{d}_i - d_i(\boldsymbol{\varphi}) - \mu_{\mathrm{LOS}}\log\left(1+d_i(\boldsymbol{\varphi})\right) - \mu_{\mathrm{NLOS}} \qquad (42)$$

Here,

$$\mathrm{E}\left[R_{\mathrm{NLOS}}\right] = 0 \qquad (43)$$

$$\mathrm{E}\left[R_{\mathrm{NLOS}}^2\right] = \sigma_{\mathrm{LOS}}^2S^2 + \sigma_{\mathrm{NLOS}}^2 - d_i(\boldsymbol{\varphi})^2 \qquad (44)$$

and (41) becomes

$$\begin{aligned}
\xi_i(\boldsymbol{\varphi}) &= \frac{\sigma_{\mathrm{LOS}}^2\log\left(1+d_i(\boldsymbol{\varphi})\right) - \left(1+d_i(\boldsymbol{\varphi})+\mu_{\mathrm{LOS}}\right)^2}{S_{\mathrm{NLOS}}\left(1+d_i(\boldsymbol{\varphi})\right)^2} \\
&\quad + \frac{\sigma_{\mathrm{LOS}}^2\left\{2\left(\sigma_{\mathrm{LOS}}\log\left(1+d_i(\boldsymbol{\varphi})\right)\right)^2 - d_i(\boldsymbol{\varphi})^2\right\}}{S_{\mathrm{NLOS}}^2\left(1+d_i(\boldsymbol{\varphi})\right)^2} \\
&\quad + \left\{S_{\mathrm{NLOS}} - d_i(\boldsymbol{\varphi})^2\right\}\frac{\sigma_{\mathrm{LOS}}^2\log(1+d_i(\boldsymbol{\varphi}))\left\{4\sigma_{\mathrm{LOS}}^2\log(1+d_i(\boldsymbol{\varphi}))+S_{\mathrm{NLOS}}^2\right\}}{S_{\mathrm{NLOS}}^3(1+d_i(\boldsymbol{\varphi}))^2}
\end{aligned} \qquad (45)$$

REFERENCES

[1] 'Ultrawideband: High-speed, short-range technology with far-reaching effects," MultiBand OFDM Alliance SIG White Paper, Sep. 2004.

[2] F. Zafari, A. Gkelias, and K. K. Leung, "A survey of indoor localization systems and technologies," *IEEE Commun. Surveys Tuts.*, vol. 21, no. 3, pp. 2568–2599, Jul.–Sep. 2019.

[3] M. Kotaru, K. Joshi, D. Bharadia, and S. Katti, "Spotfi: Decimeterlevel localization using WiFi," *ACM SIGCOMM Comput. Commun. Rev.*, vol. 45, pp. 269–282, Oct. 2015.

[4] F. J. Gonzalez-Castano and J. Garcia-Reinoso, "Bluetooth location networks," in *Proc. IEEE Glob. Telecommun. Conf.*, 2002, pp. 233–237.

[5] W. Dargie and C. Poellabauer, *Fundamentals of Wireless Sensor Networks: Theory and Practice*. Hoboken, NJ, USA: Wiley, 2010.

[6] H. Liu, H. Darabi, P. Banerjee, and J. Liu, "Survey of wireless indoor positioning techniques and systems," *IEEE Trans. Syst., Man, Cybern., Part C (Appl. Rev.)*, vol. 37, no. 6, pp. 1067–1080, Nov. 2007.

[7] J. Xiong and K. Jamieson, "ArrayTrack: A fine-grained indoor location system," in *Proc. 10th USENIX Symp. Networked Syst. Des. Implementation*, 2013, pp. 71–84.

[8] Z. Yang, Z. Zhou, and Y. Liu, "From RSSI to CSI: Indoor localization via channel response," *ACM Comput. Surv.*, vol. 46, no. 2, Nov. 2013, Art. no. 25.

[9] S. R. Jondhale, R. Maheswar, and J. Lloret, *Received Signal Strength Based Target Localization and Tracking Using Wireless Sensor Network* (EAI/Springer Innovations in Communication and Computing Series). Berlin, Germany: Springer, 2022.

[10] S. R. Jondhale and R. S. Deshpande, "Tracking target with constant acceleration motion using Kalman filtering," in *Proc. Int. Conf. Adv. Commun. Comput. Technol.*, 2018, pp. 581–587.
[11] F. Zafari, I. Papapanagiotou, and K. Christidis, "Microlocation for Internet-of-Things-equipped smart buildings," *IEEE Internet Things J.*, vol. 3, no. 1, pp. 96–112, Feb. 2016.
[12] A. Yassin et al., "Recent advances in indoor localization: A survey on theoretical approaches and applications," *IEEE Commun. Surveys Tuts.*, vol. 19, no. 2, pp. 1327–1346, Apr.–Jun. 2017.
[13] H.-B. Li, R. Miura, H. Nishikawa, T. Kagawa, and F. Kojima, "Proposals and implementation of high band IR-UWB for increasing propagation distance for indoor localization," *IEICE Trans. Fundam. Electron., Commun. Comput. Sci.*, vol. E101.A, no. 1, pp. 185–194, Jan. 2018.
[14] M. Horiba, E. Okamoto, T. Shinohara, and K. Matsumura, "An accurate indoor-localization scheme with NLOS detection and elimination exploiting stochastic characteristics," *IEICE Trans. Commun.*, vol. 98, no. 9, pp. 1758–1767, Sep. 2015.
[15] K. Fukuda and E. Okamoto, "Performance improvement of IMR-based NLOS detection in indoor ultra wide-band TOA localization," *IEICE Trans. Fundamentals*, vol. 95, no. 10, pp. 1658–1666, Oct. 2012.
[16] J. Kulmer et al., "Using DecaWave UWB transceivers for high-accuracy multipath-assisted indoor positioning," in *Proc. IEEE Int. Conf. Commun. Workshops*, 2017, pp. 1239–1245.
[17] K. Witrisal and P. Meissner, "Performance bounds for multipath-assisted indoor navigation and tracking (MINT)," in *Proc. IEEE Int. Conf. Commun.*, 2012, pp. 4321–4325.
[18] E. Leitinger, F. Meyer, P. Meissner, K. Witrisal, and F. Hlawatsch, "Belief propagation based joint probabilistic data association for multipath-assisted indoor navigation and tracking," in *Proc. Int. Conf. Localization GNSS*, 2016, pp. 1–6.
[19] H.-B. Li, K. Takizawa, and F. Kojima, "Accelerating outdoor UWB — Domestic regulation transition and standardization within IEEE 802.15," *IEICE Trans. Fundamentals*, vol. E103-A, no. 1, pp. 269–277, Jan. 2020.
[20] J. Schroeder, S. Galler, K. Kyamakya, and K. Jobmann, "NLOS detection algorithms for ultra-wideband localization," in *Proc. 2007 4th Workshop Positioning, Navigation Commun.*, 2007, pp. 159–166.
[21] K. Yu, K. Wen, Y. Li, S. Zhang, and K. Zhang, "A novel NLOS mitigation algorithm for UWB localization in harsh indoor environments," *IEEE Trans. Veh. Technol.*, vol. 68, no. 1, pp. 686–699, Jan. 2019.
[22] J. Borrás, P. Hatrack, and N. B. Mandayam, "Decision theoretic framework for NLOS identification," in *Proc. IEEE Veh. Technol. Conf.*, 1998, pp. 1583–1587.
[23] A. Lakhzouri, E. S. Lohan, R. Hamila, and M. Renfors, "Extended Kalman filter channel estimation for line-of-sight detection in WCDMA mobile localization," *EURASIP J. Adv. Signal Process.*, vol. 2003, no. 13, pp. 1–1, Dec. 2003.
[24] I. Guvenc, C. C. Chong, F. Watanabe, and H. Inamura, "NLOS identification and weighted least-squares localization for UWB systems using multipath channel statistics," *EURASIP J. Adv. Signal Process.*, vol. 2008, no. 1, pp. 1–14, Jan. 2008.
[25] S. Sczyslo, J. Schroeder, S. Galler, and T. Kaiser, "Hybrid localization using UWB and inertial sensors," in *Proc. Int. Conf. Ultra-Wideband*, 2008, pp. 89–92.
[26] P. Petrus, "Robust Huber adaptive filter," *IEEE Trans. Signal Process.*, vol. 47, no. 4, pp. 1129–1133, Apr. 1999.
[27] G. L. Sun and W. Guo, "Bootstrapping M-estimators for reducing errors due to non-line-of-sight (NLOS) propagation," *IEEE Commun. Lett.*, vol. 8, no. 8, pp. 509–510, Aug. 2004.
[28] R. Casas, A. Marco, J. J. Guerrero, and J. Falcó, "Robust estimator for non-line-of-sight error mitigation in indoor localization," *EURASIP J. Adv. Signal Process.*, vol. 2006, no. 1, pp. 1–8, Jan. 2006.
[29] S. Zhang, S. Gao, and G. Wang, "Robust NLOS error mitigation method for TOA-based localization via second-order cone relaxation," *IEEE Commun. Lett.*, vol. 19, no. 12, pp. 2210–2213, Dec. 2015.
[30] S. Venkatesh and R. M. Buehrer, "NLOS mitigation using linear programming in ultrawideband location-aware networks," *IEEE Trans. Veh. Technol.*, vol. 56, no. 5, pp. 3182–3198, Sep. 2007.
[31] S. Tomic and M. Beko, "A bisection-based approach for exact target localization in NLOS environments," *Signal Process.*, vol. 143, pp. 328–335, Feb. 2018.
[32] Y. Qi, H. Kobayashi, and H. Suda, "Analysis of wireless geolocation in a non-line-of-sight environment," *IEEE Trans. Wireless Commun.*, vol. 5, no. 3, pp. 672–681, Mar. 2006.
[33] J. Riba and A. Urruela, "A non-line-of-sight mitigation technique based on ML-detection," in *Proc. IEEE Int. Conf. Acoust., Speech, Signal Process.*, 2004, pp. ii–153.
[34] X. Li, "An iterative NLOS mitigation algorithm for localization in sensor networks," in *Proc. 15th IST Mobile Wireless Commun. Summit*, 2006, pp. 1–5.
[35] E. Arias-de-Reyna and P. M. Djuric, "Indoor localization with range-based measurements and little prior information," *IEEE Sensors J.*, vol. 13, no. 5, pp. 1979–1987, May 2013.
[36] I. Sharp, K. Yu, and Y. J. Guo, "GDOP analysis for localization system design," *IEEE Trans. Veh. Technol.*, vol. 58, no. 7, pp. 3371–3382, Sep. 2009.
[37] M. Tahsin, S. Sultana, T. Reza, and M. Hossam-E-Haider, "Analysis of DOP and its preciseness in GNSS localization," in *Proc. Int. Conf. Elect. Eng. Inf. Commun. Technol.*, 2015, pp. 1–6.
[38] N. Rajagopal, S. Chayapathy, B. Sinopoli, and A. Rowe, "Beacon placement for range-based indoor localization," in *Proc. Int. Conf. Indoor Localization Indoor Navigation*, 2016, pp. 1–8.
[39] W.-Y. Liu, E.-S. Wang, Z.-J. Chen, and L. Wang, "An improved DV-hop localization algorithm based on the selection of beacon nodes," *J. Convergence Inf. Technol.*, vol. 5, no. 9, pp. 157–164, Nov. 2010.
[40] I. Guvenc and C.-C. Chong, "A survey on TOA based wireless localization and NLOS mitigation techniques," *IEEE Commun. Surveys Tuts.*, vol. 11, no. 3, pp. 107–124, Jul.–Sep. 2009.
[41] K. W. Cheung, H. C. So, W.-K. Ma, and Y. T. Chan, "Least squares algorithms for time-of-arrival-based mobile location," *IEEE Trans. Signal Process.*, vol. 52, no. 4, pp. 1121–1128, Apr. 2004.
[42] E. Okamoto, M. Horiba, K. Nakashima, T. Shinohara, and K. Matsumura, "Low-complexity indoor UWB localization scheme using particle swarm optimization," *Nonlinear Theory Appl., IEICE*, vol. 6, no. 2, pp. 194–206, Apr. 2015.
[43] J. J. Caffery, "A new approach to the geometry of TOA location," in *Proc. IEEE Veh. Technol. Conf.*, 2000, vol. 4, pp. 1943–1949.
[44] S. P. Hozo, B. Djulbegovic, and I. Hozo, "Estimating the mean and variance from the median, range, and the size of a sample," *BMC Med. Res. Methodol.*, vol. 5, no. 13, pp. 1–10, Apr. 2005.
[45] B. Alavi and K. Pahlavan, "Modeling of the TOA-based distance measurement error using UWB indoor radio measurements," *IEEE Commun. Lett.*, vol. 10, no. 4, pp. 275–277, Apr. 2006.
[46] S. Padhye, R. A. Sahu, and V. Saraswat, *Introduction to Cryptography*, 1st ed. Boca Raton, FL, USA: CRC Press, 2018.
[47] H. Dai, K. Li, and W. Xiao, "Relative localization algorithm based on coordinates inner product matrix-based maximum likelihood," in *Proc. Int. Conf. Comput. Sci. Appl.*, 2013, pp. 203–205.
[48] L. V H.. *Trees, Detection Estimation and Modulation Theory, Part 1 Detection, Estimation, and Filtering Theory*, 2nd ed. Hoboken, NJ, USA: Wiley, 2013.
[49] C. Chang and A. Sahai, "Estimation bounds for localization," in *Proc. 1st Annu. IEEE Commun. Soc. Conf. Sensor Ad Hoc Commun. Netw.*, 2004, pp. 415–424.
[50] T. Jia and R. M. Buehrer, "A new Cramer–Rao lower bound for TOA-based localization," in *Proc. IEEE Mil. Commun. Conf.*, 2008, pp. 1–5.
[51] "UWB RTLS starter kit," 2019. [Online]. Available: www.git-inc.com/wordpress/en/?page_id=7

KEIGO ISHIDA received B.E. and M.E. degree in electrical and mechanical engineering from the Nagoya Institute of Technology, Nagoya, Japan, in 2019. He is currently engaged in engine control development with the Automotive Manufacturing Industry. His research interests included wireless communication technology and machine learning in indoor localization systems, as a student.

EIJI OKAMOTO (Member, IEEE) received the B.E., M.S., and Ph.D. degrees in electrical engineering from Kyoto University, Kyoto, Japan, in 1993, 1995, and 2003, respectively. In 1995, he joined Communications Research Laboratory, Japan. He is currently an Associate Professor with the Nagoya Institute of Technology, Nagoya, Japan. In 2004, he was a Guest Researcher with Simon Fraser University, Burnaby, BC, Canada. His research interests include wireless technologies, mobile communication systems, wireless security, and satellite communications. He was the recipient of the Young Researchers Award in 1999 from IEICE, and FUNAI Information Technology Award for Young Researchers in 2008.

HUAN-BANG Li received the B.E. degree from Northern Jiao Tong University, Beijing, China, in 1986, the M.E. and D.E. degrees from the Nagoya Institute of Technology, Nagoya, Japan, in 1991 and 1994, respectively. Since then, he has been with CRL, reshuffled to NICT since 2004, and is currently a Chief Senior Researcher of NICT. His research interests include mobile satellite communication, ultra-wideband (UWB), and D2D Networks. Since 2010, he has been a Visiting Professor with the University of Electro-Communications, Tokyo, Japan. He has authored a book *Block-coded modulations using Viterbi decoding* (in Japanese) in 1999 and coauthored a book *Wireless Body Area Network* in 2010. He was the recipient of the Young Engineer Award and Excellent Paper Award of IEICE respectively, in 1996 and 1998, Distinguished Patent Award of the Ministry of Science and Technology Agency in 2000, and IEEE-SA Standards Board acknowledges with appreciation in 2012 and 2018, respectively.